REGULAR PAPER

Nanosecond laser induced energetic ion formation from a nanoparticle: The origin of ion detection loss in a single particle mass spectrometry

Yongsuk Oh[1], Riyan Zahaf[1], Michael R. Zachariah[2], and Donggeun Lee[1*]

[1]School of Mechanical Engineering, RIMT, Pusan National University, Busan 609-735, Korea
[2]Department of Mechanical Engineering and Department of Chemistry and Biochemistry, University of Maryland, College Park, MD 20742, U.S.A.
E-mail: donglee@pusan.ac.kr

Here we study the interaction of a nanosecond laser pulse with a nanoparticle to explore the mechanism of energetic ion formation and in particular the particle size dependence. Multiphoton ionization and the subsequent electron impact ionization accompanied by inverse Bremsstrahlung process are determined appropriate for generation of multiple charged ions. The Coulomb expansion of a positive ion cloud is then calculated with molecular dynamics simulations, resulting in temporal evolution of ions, a radial distribution of kinetic energy of ions, and size-dependency of the ion kinetic energy. A mass spectrum peak of ion simulated by the present model is found comparable to the experimental data. Alternatively, a direct measurement of kinetic energy is also explained by the model. © 2014 The Japan Society of Applied Physics

1. Introduction

Recent advances in single particle mass spectrometry (SPMS) has been used to obtain both the size and composition of a single nanoparticle from a single measurement.[1–3] This offers the opportunity to probe in some detail reactivity of nanoparticles in the absence of a substrate, as for example, the solid-state reaction kinetics inside a nanoparticle,[4] size-resolved surface reaction kinetics,[5] and the origins of environmental particles.[6] However a truly quantitative analysis requires an understanding of ion production and detection in the mass-spectrometer. In particular a recent study[3] has pointed to a complication whereby the velocity distribution of laser-induced ions is dependent on particle size and thus the ion-detection efficiency in a mass-spectrometer is biased by particle size. One option is to understand the bias sufficiently to make the appropriate corrections. The other is to circumvent the problem, by for example designing a new ion optics to maximize ion-transport[7] or generating less energetic ions.

We begin with a qualitative review of the physical process under consideration. When a femto-second intense laser pulse ($>10^{15}\,\mathrm{W\,cm^{-2}}$) irradiates a gas cluster,[8,9] energetic ions up to 1–100 keV are generated, along with more energetic electrons of 0.01 to 1 MeV, leading to a formation of nanoplasma. The dynamics and energetics of the ions and electrons have been explained qualitatively by a nanoplasma model consisting of tunneling ionization, hot electron-impact ionization, resonant heating of electrons, and hydrodynamic expansion of ions and electrons.[8] On the other hand, the use of a nanosecond laser ($<10^{11}\,\mathrm{W\,cm^{-2}}$) produces less energetic ions of 1–100 eV.[10,11] Under these conditions photofragmentation[10] and Coulomb explosion[11] were proposed as a potential mechanism, though any detail quantitative modeling has not been reported.

In contrast to the extensive studies on gas cluster ionization, considerable less attention has been focused on the fundamental ionization behavior of nanosecond laser-particle interaction. In part this is due to the relative newness of interest in single particle mass spectrometry but also because of some technical challenges: 1) much less detection efficiency of nanoparticles due to their low concentration at the laser focus,[12–14] 2) a wide size distribution of particles

(10–300 nm) making it difficult to collect statistically meaningful data at a particular particle size.[3–5] To the best of our knowledge, there is only one report[15] that focuses to do this application and involves a model of the hydrodynamic expansion of the plasma.[16] The hydrodynamic expansion mechanism conflicts with the Coulomb explosion conjecture. The former argues that the expansion is driven by pressure forces while the latter argues that the ion repulsion drives the expansion.

The objective of this study is to explore in more detail the possible mechanism underlying the formation of particle size-dependent energetic ions, through a direct measurement and numerical simulation of the ionization process. The Coulomb expansion of a positive ion cloud is simulated with molecular dynamics simulations, resulting in a temporal evolution of ions, a radial distribution of ion kinetic energies, and the particle size-dependency of the ion kinetic energy. With this information we are able to obtain a simulated mass-spectrum of the Na ion and compare it with experimental data.

2. Experiment

As a model system, NaCl aerosol nanoparticles are generated in the size range of 30–300 nm by a conventional spray drying process.[3,4] The aerosol particles are fed into the SPMS consisting of an aerodynamic lens inlet, a source region for particle-to-ion conversion with a free-firing frequency-doubled pulsed Nd:YAG laser, a 1-m-long linear time-of-flight (TOF) tube and a microchannel plate (MCP) detector, as depicted in Fig. 1. Aerosols are tightly focused to a sub-millimeter beam, and then ionized by an intense pulse of the laser operating at 10 Hz, 532 nm in wavelength, 5 ns of duration time, and $3 \times 10^{10}\,\mathrm{W\,cm^{-2}}$ of laser fluence at the focus. Details of the instrumentation are described elsewhere.[3,7]

The laser beam was initially vertically polarized. By using a half-wave plate, the polarization direction was rotated to 45 and 90° (horizontal), in an effort to elucidate the nature of ionization in terms of laser-ion or laser-electron coupling. More than 500 NaCl particles were analyzed by the SPMS at each polarization direction. It is interesting to note that there is no apparent effect of polarization angle on total peak intensity and profile. This observation for single particle ionization using a ns laser pulse is in marked contrast to the
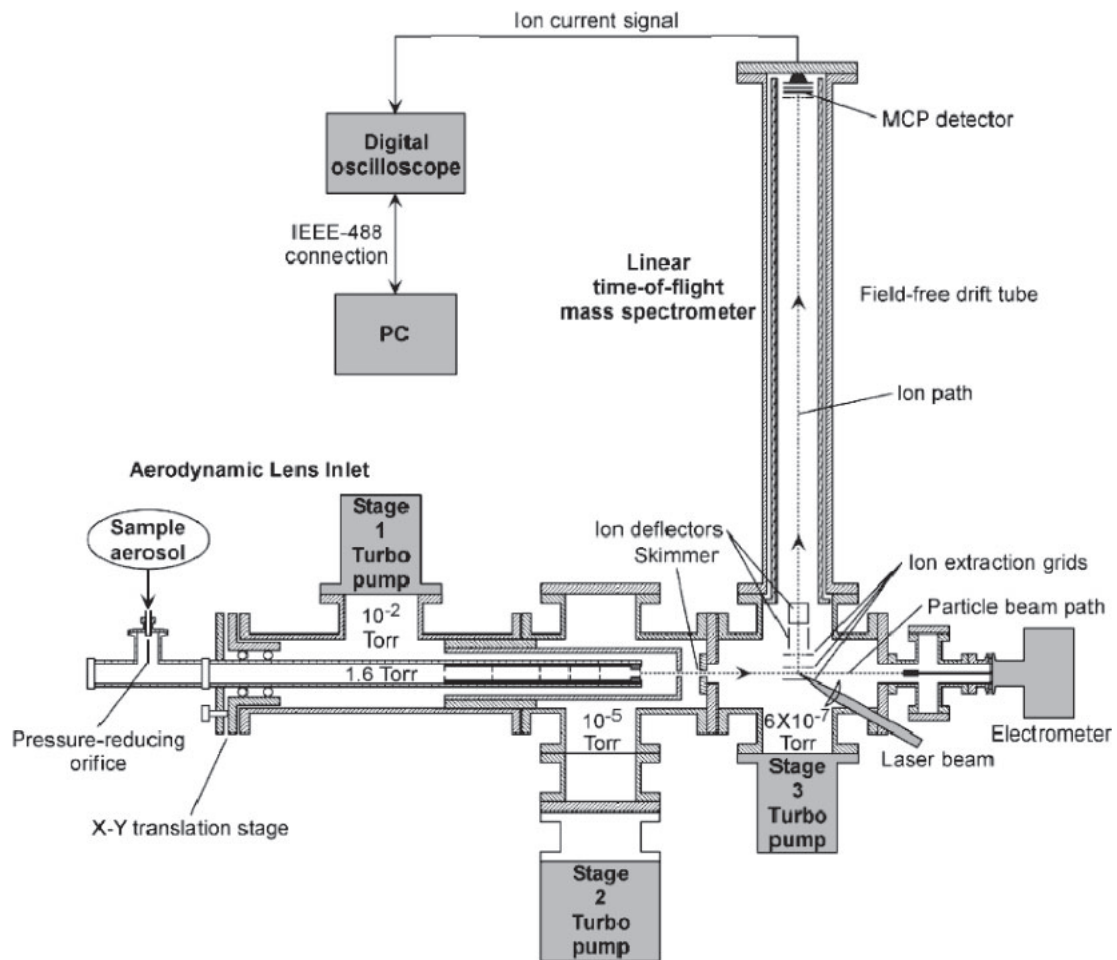
Fig. 1. Schematic of single particle mass spectrometry.

case of a fs laser ionization of gas clusters:[17] a strong polarization-angle dependence of average ion energy when Xe clusters are irradiated by a fs laser pulse with $1.3 \times 10^{16}\,\mathrm{W\,cm^{-2}}$. Hence, it is speculated that the ionization in part or expansion process is essentially isotropic.

Figure 2 shows typical mass spectra of 70 nm NaCl particles consisting of four major peaks of singly- and doubly-charged ions (Na^+, Cl^+, Na^{2+}, Cl^{2+}), and two minor peaks of chlorine isotope (Cl_{37}^+ and Cl_{37}^{2+}). Because the salt NP's, which are hygroscopic, are generated from water atomization, and then dried, a water signature is occasionally observed in the mass spectrum. The spectrum clearly shows that the peak shapes are not symmetric and have a tail on the low-mass side of the peak. Ion trajectory simulations[3] show that this behavior results from the different flight distances traveled by ions that when created are ejected either away or toward the MCP. Those that were ejected away from the MCP travel some distance in the ion-extraction region, before being turned around by the field. Those with higher energy travel further before being turned around so that those ions that happen to be ejected away from the MCP experience a temporal focusing much like a reflectron configuration which narrows the arrival time.[2–4,7] On the other hand, those ions that are ejected toward the MCP have arrival times that reflect their initial kinetic energies along with those ions that are ejected off-axis and collect by the field. These ions are responsible for the long tail shown at the low mass side of
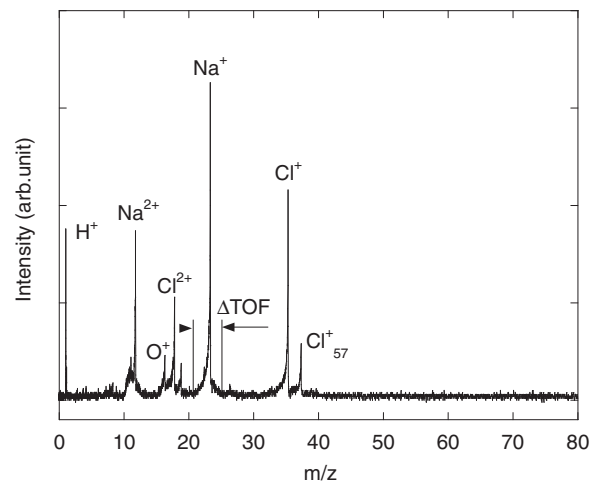
Fig. 2. Typical mass spectrum of a 70 nm NaCl nanoparticle.

each mass peak. Thus the full width of a peak, as indicated by ΔTOF in Fig. 2, is a measure of the maximum kinetic energy ($E_{k,max}$) of ions. Using the theoretical relationship for sodium ion in the present condition $[E_{k,max}\,(\mathrm{eV}) = 4302 \cdot q^2 \Delta\mathrm{TOF}\,(\mu s)^2$: q is number of multiple charge]. $E_{k,max}$ was estimated as a function of particle size by size selecting particles with a differential mobility analyzer[3,7] (DMA; TSI). Figure 3
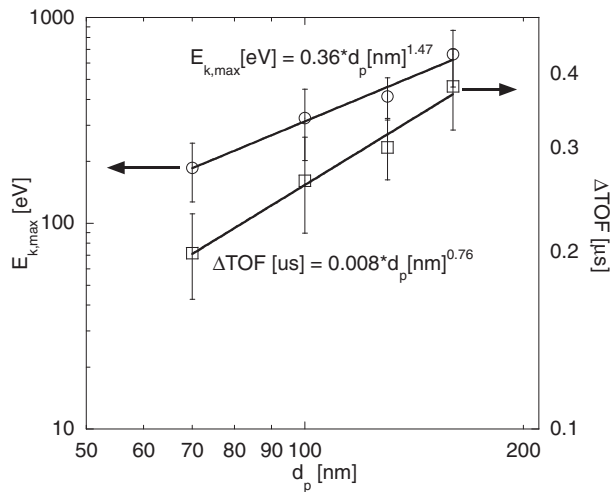
Fig. 3. Power dependences of maximum kinetic energy and difference in TOF on the particle size.
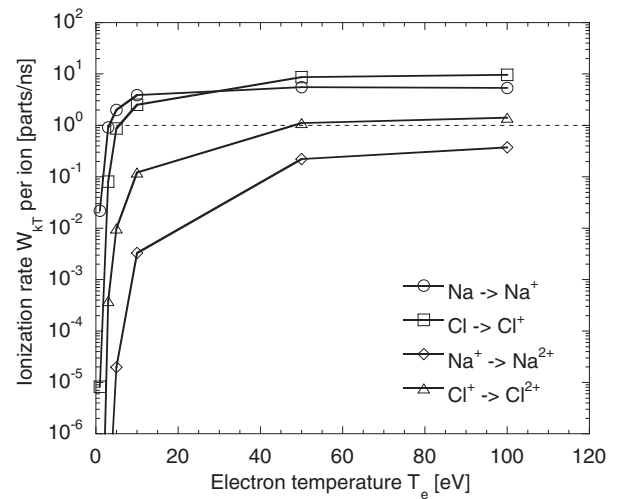
Fig. 4. Collision ionization rate of ions and atoms at solid density for 70 nm NaCl particle.

shows the first experimental measurement of $E_{k,max}$ vs particle size (d_p). It is quite clear from this result that bigger particles produce more energetic ions. The size dependence can be fitted to a power law in particle size with a measured exponent of 1.47 ($E_{k,max} \propto d_p^{1.47}$) which is reasonably close to the predicted value[3] of 1.64.

As previously mentioned it is well known that irradiation of gas clusters with femtosecond[8–11,16,18] or nanosecond[19–21] lasers results in the production of multiple charged ions, However the fact that a nanosecond laser with moderate fluencies (3×10^{10} W cm^{-2}) can produce such high energy ions from nanoparticles is a new and unexpected result. Of particular interest is to note that the values of ion kinetic energy are well above the values predicted by the hydrodynamic model proposed by Zhou et al.[15] The other major difference with gas-cluster is the lack of any molecular ions (e.g., $(NaCl)_x^+$, Na_2^+, and Cl_2^+ i) observed from nanoparticles. The rest of this paper is devoted to a plausible mechanism of the formation of size-dependent energetic ions from nanoparticles.

3. Theoretical background

Under the typical operating condition of the SPMS, positive ions and electrons are generated in the absence of negative ions because the laser intensity is several orders-of-magnitude higher than ionization potentials and binding energies of most ions.[2–6] Given that the photon energy of laser pulse is well below the ionization threshold, the ionization mechanism has been attributed to multiphoton processes (MPI). To assign a likely mechanism, we estimate the Keldysh parameter γ ($= \omega_0 \sqrt{2E_{IP} m_e}/eE_0$) where ω_0 is laser frequency, m_e is electron mass, E_{IP} is ionization potential, and E_0 is electric field strength of the laser. For Na+ ions ($E_{IP} = 5.14$ eV), the parameter γ is ca. 75, much larger than unity, suggesting that the field ionization (above threshold ionization (ATI) or tunneling ionization) cannot occur.[8,16,10–21]

For a direct ionization and for our given wavelength (532 nm), a four-photon ionization is necessary for NaCl. The ionization rate $P(I)$ (parts cm^{-3} s) is obtained by[22]

$$P(I) = \sigma_4 \left(\frac{I}{\hbar\omega} \right)^4 N_s, \qquad (1)$$

where the cross section, $\sigma_4 = 2 \times 10^{-114}$ cm^8 s^3, laser intensity, $I = 3 \times 10^{10}$ W cm^{-2}, the atomic density, $N_s = 8.99 \times 10^{22}$ parts cm^{-3}, and the term "parts" denotes number of ions or electrons. Though high density of ions, ca. 3.65×10^{16} parts cm^{-3} is created in a 5 ns pulse the ionization efficiency is quite small $\sim 4 \times 10^{-7}$. To produce the doubly ionized (Na^{2+} or Cl^{2+}) would require more than ten photons for direct optical ionization, and given the power dependence the yield would be miniscule. We can thus safely conclude that MPI cannot be responsible for the generation of multiple charged ions.

Next we consider a qualitative model proposed for gas cluster ionization with a nanosecond laser.[19–21] Free electrons of low energy generated by MPI are likely caged in the gas cloud, forming a nanoplasma at the beginning of the laser pulse, which are rapidly heated by the laser field through the inverse bremsstrahlung (IBS) process. When the electrons acquire sufficient energy over the ionization potential (IP) of the neutrals or the ions, electron impact ionization (EII) can take place to produce higher-charged ions. The rate of EII per ion (W_{kT}), in unit of parts s^{-1}, is estimated by the semi-empirical formula by Lotz[23] as

$$W_{kT} = 6 \times 10^{-8} n_e q_i \left(\frac{13.6 eV}{E_{IP}} \right)^{3/2} \left(\frac{E_{IP}}{T_e} \right)^{1/2}$$
$$\times \exp\left(\frac{E_{IP}}{T_e} \right) \int_{E_{IP}/T_e}^{\infty} \frac{e^{-x}}{x} \, dx, \qquad (2)$$

where electron density n_e is approximated to the ion density n_i of 3.65×10^{16} parts cm^{-3} right after the MIP process, q_i is number of equivalent electrons in the outermost shell of ions or neutrals, T_e is mean electron energy in eV, and the integral term is numerically calculated. Figure 4 shows the calculated rate of ionization (EII) as a function of electron temperature and indicates a very strong non-linear function on electron energy. This calculation was made for electrons and ions at the initial density (3.65×10^{16} parts cm^{-3}). Accounting for the electron avalanche during this process as well as rapid

Table I. Heating rate per electron by IBS process at different electron temperatures.

T_e (eV)	dT_e/dt per electron (eV/s)	
	at solid density of electrons	at initial density of electrons
6	1.39×10^{13}	4.01×10^7
20	3.45×10^{12}	8.25×10^6
50	1.40×10^{12}	2.30×10^6
100	6.39×10^{11}	8.71×10^5
500	8.63×10^{10}	8.99×10^4

Fig. 5. Spherical coordinate system for an ion cloud.

heating as shown below, the EII process would appear to be the likely mechanism responsible for generation of doubly-charged ions.

Next we consider electron heating by the IBS process. Provided that laser pulse energy is absorbed primarily by free electrons, the heating rate per electron is given by[8,19,20] $dE/dt = \nu U_p$, where U_p ($= 9.3 \times 10^{-14}I\lambda^2$) is the ponderomotive potential in eV in which I is laser intensity in W cm^{-2} and λ is laser wavelength in μm. The electron–ion collision frequency ν in Hz is given by $\nu = 2.9 \times 10^{-6}(Zn_e/T_e^{3/2})\ln\Lambda$, where Z is charging number of ions and $\ln\Lambda$ is the standard Coulomb logarithm. Table I lists the heating rate per electron estimated as a function of T_e, for two limiting cases of free electrons existing at solid density (8.99×10^{22} parts cm^{-3}) and the initial density (3.65×10^{16} parts cm^{-3}). The EII process should greatly increase the electron density (see Fig. 4), which would turn on the IBS process, so as to heat the electrons up to ~14 keV within 1 ns. However, while electrons become hotter, the collision frequency and the resultant heating rate are both greatly decreased, suggesting that the electron energy is limited, probably below 1 keV (refer to Table I).

Next we consider behavior of electrons and ions during the expansion process following or accompanied by the electron heating. According to Ditmire et al.'s nanoplasma model[8,18] and a more advanced hydrodynamic model,[16] most electrons never escape from the plasma, and undergo a rapid hydrodynamic expansion together with positive ions. Neither model however can explain their own experimental finding of angular anisotropic (laser-polarization dependent) energies and the resultant spectral peaks of electrons and ions[17] upon the femto second laser irradiation on gas clusters.

In contrast to the case of femto-second laser experiments on gas clusters, our experiment revealed that ion yield is independent of the laser polarization, and thus more consistent with the Coulomb explosion postulated as a mechanism for the formation of energetic ions (<100 eV) during nanosecond laser irradiation to gas clusters.[19–21] Of particular interest is to note the current nanosecond laser induces an electrostatic barrier potential[24] U_b as low as ~1.5 eV around an ion, much lower than the present electron energy. This suggests that most of the electrons exceed the attraction barrier from a localized ion so that they can move to and accumulate around the surface of the plasma. Then, the outermost electrons are likely forced to escape from the plasma, layer by layer until leaving a single surface layer of electrons, in response to the Coulomb repulsion exerted by the inner-layered electrons rather than the attraction by the positive ionic core. The escaping electron reduces the
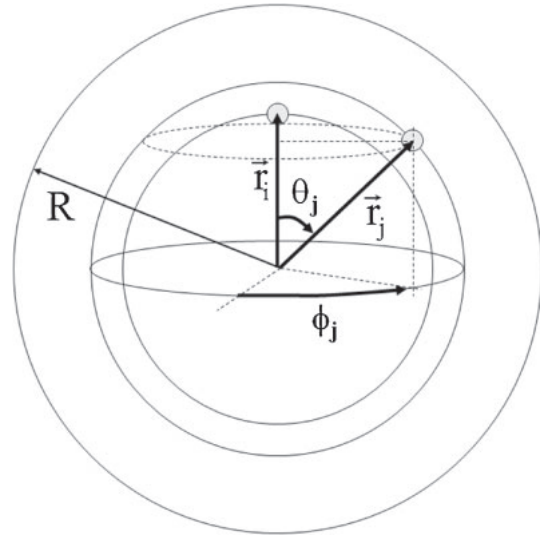
electron–ion collision frequency, and thereby degrades the EII process. This might be a possible reason for the absence of triply-charged ions in the mass spectra (see Fig. 2) despite the fact that the computed electron energy is much higher than their corresponding ionization potentials. Finally, there remains another unsolved problem, i.e., why are the ions so energetic.

4. Nuclear dynamics of positive ion cloud

To investigate the possible reason for energetic ion formation, we develop a simple molecular dynamics (MD) model under the following assumptions; 1) In the course of three parallel/sequential processes such as MPI, EII, and IBS, free electrons completely (or near so) escape from the nanoplama, leaving a spherical ion cloud, and 2) the ion cloud expands with spatially uniform density.[8] As the simple expansion of ion cloud is driven by the Coulomb repulsion between ions, the simple mechanism was called the Coulomb expansion. However, the figure of Coulomb expansion is somewhat distinct from the Coulomb explosion which requires the formation of highly-charged cluster ions. Unlike the Coulomb explosion often leaving molecular peaks in the mass spectra, the present mass spectra as shown in Fig. 2 do not show any signature of molecules. Figure 5 shows the spherical coordinate system for the MD simulation, where r_i and r_j denote the radial position vectors of the ith and the jth ions. The relative position vector between the ions is given by

$$r_{ij} = r_j \sin\theta_j \cos\phi_j \hat{\imath} + r_j \sin\theta_j \sin\phi_j \hat{\jmath} + (r_j \cos\theta_j - r_i)\hat{k}. \quad (3)$$

The differential force vector d^6F_{ij} exerted on the ith ion by the jth ion is obtained by differentiating the corresponding Coulomb potential U_{ij} as

$$U_{ij} = \frac{1}{4\pi\varepsilon_0}\frac{q_iq_j}{r_{ij}}, \quad d^6F_{ij} = -\nabla U_{ij} = \frac{1}{4\pi\varepsilon_0}\frac{q_iq_j}{r_{ij}^3}r_{ij}, \quad (4)$$

where ε_0 is vacuum permittivity, and q_i and q_j are ionic charges of the ith and jth ions. Any tangential and circumferential components of the force d^6F_{ij} are cancelled

out due to the axis symmetry, so that the net force on the ith ion $d^3\mathbf{F}_i$ by all other ions is obtained by integrating $d^6\mathbf{F}_{ij}$ over the entire volume of the sphere as

$$
\begin{aligned}
d^3\mathbf{F}_i &= \iiint d^6\mathbf{F}_{ij} \cdot \hat{k} \\
&= \iiint \frac{1}{4\pi\varepsilon_0} \frac{\rho^2\,dV_i}{r_{ij}^3} (\mathbf{r}_{ij} \cdot \hat{k})\,dV_j \\
&= \frac{\rho e}{3\varepsilon_0} r_i, \text{ or } \frac{\rho^2\,dV_i}{3\varepsilon_0} r_i,
\end{aligned}
\tag{5}
$$

where ρ and dV_j $(= r_j^2 \sin\theta_j\,d\theta_j\,d\phi_j\,dr_j)$ are charge density of ions in and the differential volume for the jth ion, respectively. Note that the net force on the ion linearly increases as radial position of the ion increases, suggesting that surface ions become most energetic. The explicit equation of the net force on any ith ion greatly reduces the overall calculation, relative to a conventional molecular dynamics simulation.

Providing initial values of the cloud radius R_0, number of ions N_s, and charge density $\rho_0 = N_s e/(4\pi/3 R_0^3)$, the acceleration of any ion is obtained from Eq. (5), and with Newton's second law we obtain the instantaneous temporally varying velocity and kinetic energy E_k of ions. Likewise, the velocity and the resultant displacement vector of the ion updates the next-step position of the ion. The Verlet algorithm is used for all time integrations with second order accuracy.[25] At the same time, the effective potential energy on the ith ion at $r = r_i$ is obtained by integrating U_{ij} over all jth ions as

$$
\begin{aligned}
d^3U_i &= \frac{1}{4\pi\varepsilon_0} \iiint \frac{\rho^2\,dV_i}{r_{ij}} r_j^2 \sin\theta_j\,d\theta_j\,d\phi_j\,dr_j \\
&= \frac{\rho^2\,dV_i}{12\varepsilon_0}(3R^2 - r_i^2),
\end{aligned}
\tag{6}
$$

where R is outer radius of the spherical ion cloud at any time. The total potential energy of the entire ion cloud U is given by integrating d^3U_i over the volume as

$$
U = \iiint d^3U_i = \frac{4}{15}\frac{\pi}{\varepsilon_0}\rho^2 R^5.
$$

The average potential energy per ion is simply obtained by dividing U by total number of ions N_s as follows and is proportional to the particle surface area:

$$
\bar{U} = \frac{U}{N_s} = \frac{3Ue}{\rho 4\pi R^3} = \frac{\rho R^2}{5\varepsilon_0}.
\tag{7}
$$

In this way, the temporal evolution of R, U, and E_k are simulated. The results indicate that the potential energy U is completely converted into kinetic energy within 100 ps, so that the average kinetic energy $\bar{E}_k$ is proportional to surface area of the original particle $(\propto R_0^2)$. It is interesting to note that the exponent of 2.0 from MD simulation is reasonably close to the experimental values of 1.47 in Fig. 3 and 1.64 from our previous work.[3] Moreover, the local kinetic energy of ions $E_k(r_i)$ is spatially not uniform; $E_k(r_i)/E_{k,\max} = r_i^2/R^2$ along with $\bar{E}_k = E_{k,\max} 3/5$, in response to the r_i dependence of d^3U_i [see Eq. (6)]. This spatial dependence of E_k, together with the previous finding[3] of detection efficiency $DE = 0.16/E_k$, indicates that most energetic surface ions will be underrepresented relative to less energetic inner ions in an
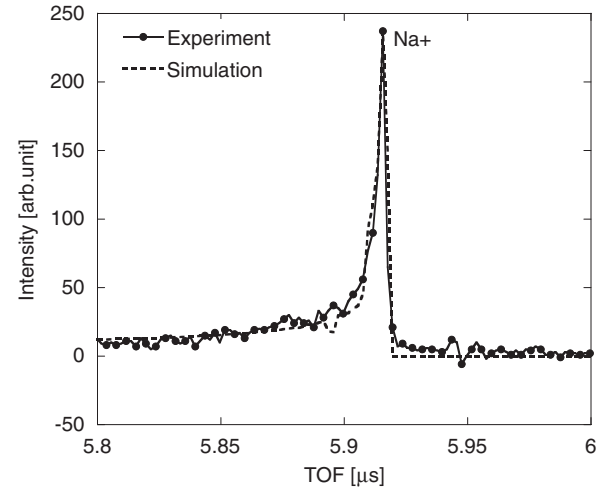
Fig. 6. Simulation of mass spectral peak profile of sodium ion from a 70 nm NaCl particle.

experiment leading to a significant bias in the compositions of core–shell composite particles.

In Ref. 3, an ion tracing method was introduced to obtain the TOF of ions emitting at different values of E_k and θ (emitting angle with respect to the TOF axis) from which a function relationship of $\text{TOF}(E_k, \theta)$ was obtained. Recalling $E_k(r_i) = E_{k,\max} r_i^2/R^2$, it is possible to predict the TOF of every ion radially emitting from a location of r_i and θ, and determine if it will strike the MCP and be detected. Consider a differential sector of $\theta \sim \theta + \Delta\theta$ and $r_i \sim r_i + \Delta r_i$ where the number of existing ions ΔN_θ is given by $\rho 2\pi r_i^2 \sin(\theta)\Delta\theta\Delta r_i$. For an initial value of $E_{k,\max}$, a single value of TOF is calculated for the ions and then ΔN_θ times recorded in a database if the ions are detectable. This process is repeated until the entire volume of the ion cloud is scanned, resulting in a tabulation of TOFs for all detectable ions, from which a histogram of detectable ions can be constructed and actually corresponds to a single peak of a mass spectrum. In this way, a mass spectral peak of Na$^+$ is simulated for a 70 nm NaCl particle, provided $E_{k,\max} = 100$ eV. Figure 6 shows that the simulation is in excellent agreement with the experiment. The fitting parameter of $E_{k,\max}$ is a little lower than the lower limit of the measured value 170 ± 55 eV (see Fig. 3), which is probably originated from the simplification of the present model.

5. Direct measurement of ion kinetic energy

In our experiment, the strong E_k dependence of the detection efficiency hampers the detection of ions with energies higher than 1000 eV. To circumvent the problem we removed the TOF tube, so that the MCP was mounted much closer to the source thus greatly increasing the acceptance angle as depicted in Fig. 7. This external field-free setup offers a great benefit enabling E_k-independent measurement of ions, i.e., with the E_k-independent detection efficiency. In this setup, however, identification of species is impossible and hit rate of particles is significantly reduced thus precluding particle size selection.

Figure 8(a) shows a typical mass spectrum obtained in the field-free condition. The spectrum shows two broad peaks at
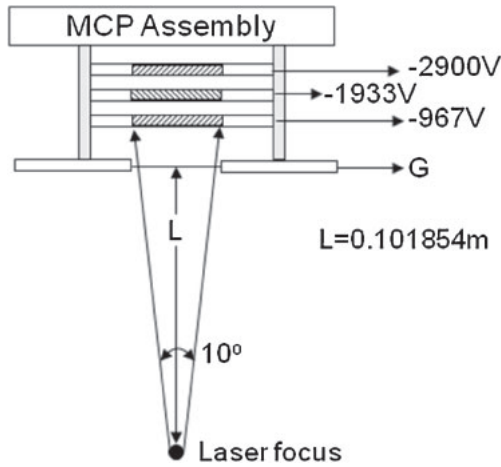
Fig. 7. Experimental setup for a direct measurement of kinetic energy of ions with the same efficiency.

Fig. 8. (a) A model prediction of mass spectrum obtained in a field-free condition. (b) Kinetic energy distribution transformed on the basis of Na.

0.84 and 2.36 µs corresponding to doubly and singly charged ions, respectively. The gray line in Fig. 8(a) results from the model simulation as follows. In the setup, the TOF of ions are simply related to the E_k or ion velocity V_i as

$$\text{TOF} = \frac{L}{V_i} = \sqrt{\frac{m_i}{2E_k}}L. \tag{8}$$

Next, a probability for ions to have an energy between E_k and $E_k + \Delta E_k$ is defined by the term of $f(E_k)\Delta E_k$ where $f(E_k)$ is called an energy distribution function. In the uniform-density one-dimensional space, the probability can be set equal to the fraction of ions (ΔN_i) existing in a sub-shell between r_i and $r_i + \Delta r_i$, relative to N_s, so that $f(E_k)\Delta E_k = \Delta N_i/N_s = 4\pi r_i^2 \Delta r_i/V_0$ where V_0 is total volume of the cloud. Then, the exact functional form of $f(E_k)$ is given by

$$f(E_k) = 3\left(\frac{r_i}{R}\right)^2 \frac{d(r_i/R)}{dE_k} = \frac{3}{2}\sqrt{\frac{E_k}{E_{k,max}}}\frac{1}{E_{k,max}}. \tag{9}$$

The intensity I in Fig. 8(a) represents a number of ion detected in a second, i.e., $I \propto dN_i/d\text{TOF}$. Since $f(E_k) \propto dN_i/dE_k$, the intensity is proportional to $f(E_k) \times dE_k/d\text{TOF}$. The term of $dE_k/d\text{TOF}$ is given from Eq. (8). Hence, the intensity I is expressed in terms of TOF as

$$I \propto f(E_k)\frac{dE_k}{d\text{TOF}} \propto \frac{\text{TOF}_{min}^3}{\text{TOF}^4}3L, \tag{10}$$

where TOF_{min} is a minimal value of TOF exhibited by the fastest ion having $E_{k,max}$ [see Eq. (8)]. Thus Eq. (10) is used for simulation of each of ion groups such as Na^+, Cl^+, Na^{2+}, and Cl^{2+} with the constraint of $\text{TOF} \geq \text{TOF}_{min}$ and proper guesses of $E_{k,max}$ for each groups. According to the present model in Sect. 4, there is no reason for ions of Na^+ and Cl^+ to have different values of $E_{k,max}$ as long as they are mixed together right before their expansion. Also this is supported by the measured relative composition close to theoretical value.[3,4] Given 320 and 3.2 keV for singly- and doubly-charged groups, respectively, the experimental profile is reasonably predicted by the present model as presented in Fig. 8(a). The value of 320 eV for singly charged ions still lies in the observed kinetic energy in Fig. 3.

Another thing to note is that the electron peak near zero TOF is so low relative the peaks of ions, suggesting that most
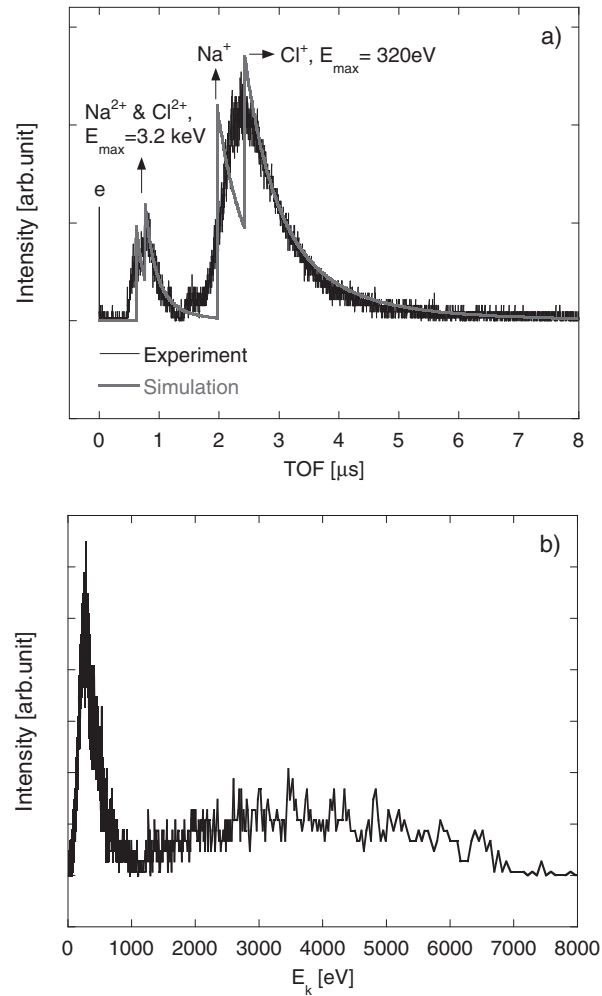
of electrons are not detected, presumably due to the negative voltage barrier supplied to MCP (see Fig. 7). Regarding the value of −967 V on the first plate, the kinetic energy of electrons is lower than 1 keV. Here it is very interesting to see in Fig. 8(b) that the E_k of ions reaches 7 keV. This implies that ions follow another route to have such a high kinetic energy. Such decoupling of ions and electrons make the hydrodynamic model questionable in the present condition. Figure 8(b) was simply obtained by converting TOF in Fig. 8(a) to E_k by using Eq. (8).

6. Conclusions

Throughout this paper, four sequential/parallel processes were proposed as a mechanism for the formation of energetic ions with multiple charges revealed by single particle mass spectrometry. The MPI process initiates ionization of particles to produce free electrons that would be subjected to further process of EII and IBS process, leading to generation of doubly-charged ions. Raising a possibility of electron–ion decoupling during/after laser irradiation, we developed a simple code to examine the nuclear dynamics of positive ions. As a result, the model predicted reasonably well the mass spectral peak observed by experiment. Further experiment made in a field-free condition revealed that kinetic energy of ions reached 7 keV, far beyond the

prediction by hydrodynamic models. Therefore, we would conclude that there still open a possibility that the Coulomb expansion is responsible for generation of energetic ions.

Acknowledgements

1) C. A. Noble and K. A. Prather, Mass Spectrom. Rev. **19**, 248 (2000).
2) W. D. Reents and Z. Ge, Aerosol Sci. Technol. **33**, 122 (2000).
3) D. Lee, K. Park, and M. R. Zachariah, Aerosol Sci. Technol. **39**, 162 (2005).
4) R. Mahadevan, D. Lee, H. Sakurai, and M. R. Zachariah, J. Phys. Chem. A **106**, 11083 (2002).
5) D. Lee, A. Miller, D. Kittelson, and M. R. Zachariah, J. Aerosol Sci. **37**, 88 (2006).
6) K. Park, D. Lee, A. Rai, D. Mukherjee, and M. R. Zachariah, J. Phys. Chem. B **109**, 7290 (2005).
7) S.-W. Cho and D. Lee, Rapid Commun. Mass Spectrom. **21**, 3286 (2007).
8) T. Ditmire, T. Donnelly, A. M. Rubenchik, R. W. Falcone, and M. D. Perry, Phys. Rev. A **53**, 3379 (1996).
9) M. H. R. Hutchinsons, T. Ditmire, E. Springate, J. W. G. Tisch, Y. L. Shao, M. B. Mason, N. Hay, and J. P. Marangos, Philos. Trans. R. Soc. London, Ser. A **356**, 297 (1998).
10) Z. Y. Chen, C. D. Cogley, J. H. Hendricks, B. D. May, and A. W. Castleman, J. Chem. Phys. **93**, 3215 (1990).
11) J. T. Snodgrass, C. M. Roehl, and M. T. Bowers, Chem. Phys. Lett. **159**, 10 (1989).
12) K.-S. Lee, S.-W. Cho, and D. Lee, J. Aerosol Sci. **39**, 287 (2008).
13) K.-S. Lee, S. Kim, and D. Lee, J. Aerosol Sci. **40**, 1010 (2009).
14) D. B. Kane, B. Oktem, and M. V. Johnston, Aerosol Sci. Technol. **34**, 520 (2001).
15) L. Zhou, K. Park, H. M. Milchberg, and M. R. Zachariah, Aerosol Sci. Technol. **41**, 818 (2007).
16) H. M. Milchberg, S. J. McNaught, and E. Parra, Phys. Rev. E **64**, 056402 (2001).
17) E. Springate, N. Hay, J. W. G. Tisch, M. B. Mason, T. Ditmire, M. H. R. Hutchinson, and J. P. Marangos, Phys. Rev. A **61**, 063201 (2000).
18) T. Ditmire, Phys. Rev. A **57**, R4094(R) (1998).
19) X. Luo, D. Niu, X. Kong, L. Wen, F. Liang, K. Pei, B. Wang, and H. Li, Chem. Phys. **310**, 17 (2005).
20) D. Niu, H. Li, F. Liang, L. Wen, X. Luo, B. Wang, and H. Qu, J. Chem. Phys. **122**, 151103 (2005).
21) X. Kong, X. Luo, D. Niu, and H. Li, Chem. Phys. Lett. **388**, 139 (2004).
22) B. C. Stuart, M. D. Feit, S. Herman, A. M. Rubenchik, B. W. Shore, and M. D. Perry, Phys. Rev. B **53**, 1749 (1996).
23) W. Lotz, Z. Phys. **232**, 101 (1970).
24) I. Last and J. Jortner, J. Chem. Phys. **120**, 1336 (2004).
25) M. P. Allen and D. J. Tildesley, *Computer Simulation of Liquids* (Clarendon Press, Oxford, U.K., 1987).